Balance-equation analysis of hot-carrier Bloch transport in a superlattice miniband

1992 J. Phys.: Condens. Matter 4 9375

(http://iopscience.iop.org/0953-8984/4/47/018)

J. Phys.: Condens. Matter 4 (1992) 9375–9388. Printed in the UK

Balance-equation analysis of hot-carrier Bloch transport in a superlattice miniband

X L Lei†‡, N J M Horing‡ and H L Cui‡

† Shanghai Institute of Metallurgy, Chinese Academy of Sciences, 865 Changning Road, Shanghai 200050, People's Republic of China

‡ Department of Physics and Engineering Physics, Stevens Institute of Technology, Hoboken, NJ 07030, USA

Received 11 May 1992, in final form 8 July 1992

Abstract. A systematic theoretical study of Bloch electron transport in a superlattice miniband driven by a uniform external electric field parallel to the growth axis is carried out, based upon a recent extension of the balance-equation approach to arbitrary energy bands, with a dynamic force-balance equation for the centre of mass (CM), a variable-mass particle embodying the collective motion of the electrons, and a dynamic energy-balance equation. Analyses of both steady-state transport and the transient response to a step and an impulsive electric field are made for various superlattice systems, assuming tight-binding miniband structure and using parameters appropriate for Γ-valley electrons in GaAs-based quantum-well superlattices at various lattice temperatures. In the steady-state case the drift velocity, v_d, electron temperature T_e, average inverse effective mass of the CM, and other quantities, are presented as functions of the electric field. In the transient response case they are presented as functions of time, following turn-on of the step or impulse electric field.

1. Introduction

Early interest in superlattices was motivated by the possibility of negative differential mobility for perpendicular carrier transport. About twenty years ago, Esaki and Tsu [1] proposed that a manmade one-dimensional potential structure, or a superlattice in which carriers move in a periodic potential on a scale of many lattice constants, would facilitate the observation of quantum mechanical properties of Bloch states in a new domain of physical scale. The narrow wavevector minizones and the narrow energy bands make it possible for electrons to be accelerated beyond the inflection point with moderate electric fields, leading to a negative differential conductance. However, subsequent observations of the negative differential conductance in carrier transport perpendicular to the superlattice layers have been attributed to the formation of highly localized high-field domains [2–4], rather than Bloch transport. It was not until the past few years that perpendicular carrier motion was clearly demonstrated to occur through a Bloch-type miniband state [5]. With steady improvements in the quality of semiconductor microstructures, research on superlattice vertical transport has intensified with renewed activity. Recent systematic measurements [6–8] were able to show that perpendicular negative differential mobility was observed as a bulk effect, and that

0953-8984/92/479375+14$07.50

Bloch electron conduction through the superlattice miniband is responsible for this negative differential conductance over a large range of superlattice parameters.

Following the original pioneering analysis of Esaki and Tsu [1,9], there were several Monte-Carlo calculations [10–12] on superlattice miniband transport. However, a detailed theoretical investigation, even a numerical one, to facilitate quantitative comparison with experiments, is still lacking. There remains an urgent need to establish a more sophisticated theory, preferably an analytical one, to provide ready access to theoretical explication of experimental data on perpendicular Bloch transport of carriers in a superlattice.

Recently effective-force and energy-balance equations have been derived for hot-electron Bloch transport in an arbitrary finite-width energy band [13]. These equations are extensions of the balance equations developed earlier by Lei and Ting [14] for parabolic band structures generalized to the case of carriers moving in a single realistic energy band subject to an arbitrary uniform electric field. The balance equations provide a succinct two-parameter description of hot-electron Bloch transport. We have briefly reported the application of these equations to discuss the negative differential velocity in the steady-state miniband conduction of a superlattice [15]. In this paper we will give a more detailed analysis of the perpendicular Bloch transport of carriers in a superlattice miniband for both the steady state and transient cases.

2. Effective-force and energy-balance equations

The balance equation theory of electron transport in an arbitrary energy band under the influence of a strong electric field devolves upon two parameters, the momentum of the centre of mass (CM) $\boldsymbol{P} = N\boldsymbol{p}_d$ (N is the total number of carriers) and the electron temperature T_e. The rate of change of the average drift velocity $\boldsymbol{v}_d$, and the rate of change of the internal energy h_e (per carrier) of the system, satisfy the following equations [13]:

$$\frac{d\boldsymbol{v}_d}{dt} = e\boldsymbol{E}\cdot\boldsymbol{\mathcal{K}} + \boldsymbol{A}_i + \boldsymbol{A}_p \tag{1}$$

$$\frac{dh_e}{dt} = e\boldsymbol{E}\cdot\boldsymbol{v}_d - W. \tag{2}$$

Here $\boldsymbol{\mathcal{K}}$ is the average inverse effective mass tensor, defined as

$$\boldsymbol{\mathcal{K}} = \frac{2}{N}\sum_{\boldsymbol{k}} \nabla\nabla\varepsilon(\boldsymbol{k}) f(\bar{\varepsilon}(\boldsymbol{k}), T_e) \tag{3}$$

and the drift velocity $\boldsymbol{v}_d$ is given by

$$\boldsymbol{v}_d = \frac{2}{N}\sum_{\boldsymbol{k}} \boldsymbol{v}(\boldsymbol{k}) f(\bar{\varepsilon}(\boldsymbol{k}), T_e) \tag{4}$$

in which $\varepsilon(\boldsymbol{k})$ is the zero-field single-band energy of the electron state of wavevector $\boldsymbol{k}$, and $\boldsymbol{v}(\boldsymbol{k}) \equiv \nabla\varepsilon(\boldsymbol{k})$ is the velocity function. Here we utilize a periodic zone description for the electrons, such that $\boldsymbol{k}$ and $\boldsymbol{k}+\boldsymbol{G}$ ($\boldsymbol{G}$ is a reciprocal lattice vector) represent the same state: $\varepsilon(\boldsymbol{k}+\boldsymbol{G}) = \varepsilon(\boldsymbol{k})$, and $\boldsymbol{v}(\boldsymbol{k}+\boldsymbol{G}) = \boldsymbol{v}(\boldsymbol{k})$, and the sum over

k goes over $N_L \equiv 1/\Omega$ (Ω is the volume of the unit cell) points within a volume of a Brillouin zone. In (3) and (4)

$$\bar{\varepsilon}(k) = \varepsilon(k - p_d) \tag{5}$$

and

$$f(\bar{\varepsilon}(k), T_e) = \{\exp[(\bar{\varepsilon}(k) - \mu)/T_e] + 1\}^{-1} \tag{6}$$

is the Fermi distribution function at electron temperature T_e and μ is the chemical potential, which should be determined in accordance with

$$N = 2\sum_k f(\bar{\varepsilon}(k), T_e) = 2\sum_k f(\varepsilon(k), T_e). \tag{7}$$

In (1) A_i and A_p are the frictional accelerations of the centre of mass due to impurity and phonon scatterings, respectively, and in (2) W is the energy loss rate per carrier from the electron system to the phonon system:

$$A_i = \frac{2\pi n_I}{N}\sum_{k,q}|u(q)|^2|g(k,q)|^2[v(k+q) - v(k)]\,\delta(\varepsilon(k+q) - \varepsilon(k)) \times \frac{f(\bar{\varepsilon}(k), T_e) - f(\bar{\varepsilon}(k+q), T_e)}{|\epsilon(q, \bar{\varepsilon}(k) - \bar{\varepsilon}(k+q))|^2} \tag{8}$$

$$A_p = \frac{4\pi}{N}\sum_{k,q,\lambda}|M(q,\lambda)|^2|g(k,q)|^2[v(k+q) - v(k)]\,\delta(\varepsilon(k+q) - \varepsilon(k) + \Omega_{q,\lambda}) \times \frac{f(\bar{\varepsilon}(k), T_e) - f(\bar{\varepsilon}(k+q), T_e)}{|\epsilon(q, \bar{\varepsilon}(k) - \bar{\varepsilon}(k+q))|^2}\left[n\left(\frac{\Omega_{q,\lambda}}{T}\right) - n\left(\frac{\bar{\varepsilon}(k) - \bar{\varepsilon}(k+q)}{T_e}\right)\right] \tag{9}$$

$$W = \frac{4\pi}{N}\sum_{k,q,\lambda}|M(q,\lambda)|^2|g(k,q)|^2\Omega_{q,\lambda}\,\delta(\varepsilon(k+q) - \varepsilon(k) + \Omega_{q,\lambda}) \times \frac{f(\bar{\varepsilon}(k), T_e) - f(\bar{\varepsilon}(k+q), T_e)}{|\epsilon(q, \bar{\varepsilon}(k) - \bar{\varepsilon}(k+q))|^2}\left[n\left(\frac{\Omega_{q,\lambda}}{T}\right) - n\left(\frac{\bar{\varepsilon}(k) - \bar{\varepsilon}(k+q)}{T_e}\right)\right]. \tag{10}$$

In these equations n_I is the impurity density, $\Omega_{q\lambda}$ is the frequency of the phonon of wavevector q in branch λ, $u(q)$ and $M(q\lambda)$ are the Fourier representations of the impurity potential and the electron–phonon coupling matrix element, and $n(x) = (e^x - 1)^{-1}$ is the Bose function; $\epsilon(q,\omega)$ is the dielectric function of the electrons in the random-phase approximation:

$$|\epsilon(q,\omega)|^2 = \left(1 - v_c(q)\sum_k \Pi_1^0(k,q,\omega)\right)^2 + \left(v_c(q)\sum_k \Pi_2^0(k,q,\omega)\right)^2 \tag{11}$$

where $\Pi_1^0(q,\omega)$ and $\Pi_2^0(q,\omega)$ are the real and imaginary parts of the density–density correlation function of the electron system in the absence of Coulomb interactions:

$$\Pi^0(k,q,\omega) = 2|g(k,q)|^2\frac{f(\bar{\varepsilon}(k), T_e) - f(\bar{\varepsilon}(k+q), T_e)}{\bar{\varepsilon}(k+q) - \bar{\varepsilon}(k) + \omega - i\delta}. \tag{12}$$

In (8)–(10) and (12), $g(k,q)$ is a form factor related to the electron wavefunction $\psi_k(r)$:

$$g(k,q) = \sum_{k'} \int \mathrm{d}r \mathrm{e}^{\mathrm{i}q\cdot r} \psi^*_{k'}(r)\psi_k(r). \tag{13}$$

In the steady state (1) and (2) reduce to

$$eE\cdot\mathcal{K} + A_i + A_p = 0 \tag{14}$$

$$eE\cdot v_d - W = 0. \tag{15}$$

Equation (14) indicates that in the steady state the resistive accelerations due to the impurity and phonon scatterings exactly cancel the electric-force acceleration of the centre of mass, which behaves as a particle of a charge Ne and an inverse effective mass $\mathcal{K}/N$. Equation (15) shows that in the steady state the energy supplied by the electric field is fully dissipated to the phonon system.

Because of the appearance of the centre-of-mass momentum in $\tilde{\varepsilon}(k)$, the quantities in (14) and (15), such as the averaged inverse effective mass tensor $\mathcal{K}$, the drift velocity v_d, the frictional accelerations A_i and A_p, and the energy loss rate W, are all functions of the CM momentum p_d and the electron temperature T_e. The balance equations (14) and (15) enable us to determine the steady-state values of p_d and T_e, and thus all the physical quantities, once the electric field is given. On the other hand, (1) and (2) describe the time-dependent process on a timescale that is much longer than the thermalization time of the system. In this case we can treat both p_d and T_e as time-dependent parameters, and (1) and (2) become coupled time differential equations for p_d and T_e. One can solve these equations to obtain the transient response of the system to an external electric field $E(t)$.

3. Steady-state perpendicular transport of carriers in a superlattice miniband

We assume that the conducting carriers of the superlattice are free to move in layers (x–y plane), but are subject to a periodic potential in the z direction. The single-electron state of the system can be described by a wavevector $k = (k_\parallel, k_z)$, $-\pi/d < k_z \leqslant \pi/d$ (where d is the period of the superlattice), together with a miniband index n, with the Bloch wavefunction written as $\psi_{nk}(r) \equiv \psi_{nk}(r_\parallel, z) = S^{-1/2}\exp(\mathrm{i}k_\parallel\cdot r_\parallel t)\zeta_{nk_z}(z)$ (here S is the area of the system in the x–y plane), and the eigenenergy is $\varepsilon_n(k) = \varepsilon_{k_\parallel} + \varepsilon_n(k_z)$, ($\varepsilon_{k_\parallel} = k_\parallel^2/2m$, m being the effective mass of the carrier in the underlying lattice). The envelope function $\zeta_{nk_z}(z)$ is determined by the periodic potential of the superlattice. Since we are interested in the case in which the carriers are fairly tightly bound to a single quantum well, we can use the tight-binding sum for the envelope function

$$\zeta_{nk_z}(z) = \frac{A_{nk_z}}{L^{1/2}} \sum_l \mathrm{e}^{\mathrm{i}k_z ld}\phi_n(z - ld) \tag{16}$$

where A_{nk_z} is a normalization coefficient and $\phi_n(z)$ is the single-well eigenfunction of energy ε_n for the well centred at $z = 0$, which is normalized as $\int|\phi_n(z)|^2\mathrm{d}z = d$.

Considering only nearest-neighbour overlap in the tight-binding approximation, we have the miniband energy dispersion

$$\varepsilon_n(k_z) = \varepsilon_n + (-1)^n \frac{\Delta_n}{2} \cos k_z d \tag{17}$$

with Δ_n being the bandwidth of the nth miniband, and the normalization coefficients are not much different from unity:

$$A_{nk_z} = 1 + 2\alpha_n \cos k_z d \tag{18}$$

where $\alpha_n = d^{-1} \int \phi_n^*(z)\phi_n(z-d)\mathrm{d}z$, the wavefunction overlap integral, is a small coefficient.

In further discussions we consider only the lowest miniband ($n = 1$), such that we can drop the miniband index from the above expressions, and write the electron energy as

$$\varepsilon(\boldsymbol{k}) = \varepsilon_{\boldsymbol{k}_\parallel} + \varepsilon_1(k_z) \tag{19}$$

$$\varepsilon_1(k_z) = \frac{\Delta}{2}(1 - \cos k_z d) \tag{20}$$

where we have chosen the band bottom (at $\boldsymbol{k}_\parallel = 0, k_z = 0$) as the energy origin and $\Delta \equiv \Delta_1$ denotes the miniband width.

The form factor $g(\boldsymbol{k}, \boldsymbol{q})$ can be calculated by substituting the tight-binding envelope function (16) into (13). Neglecting the small correction due to wavefunction overlap we have

$$g(\boldsymbol{k}, \boldsymbol{q}) \simeq \frac{1}{d} \int \mathrm{e}^{\mathrm{i}q_z z} |\phi(z)|^2 \mathrm{d}z \equiv g(q_z) \tag{21}$$

independent of $\boldsymbol{k}$, where $\phi(z)$ is the single-well wavefunction of the ground state.

For the energy dispersion as described by (19) the average inverse effective mass tensor $\mathcal{K}$ is diagonal with $\mathcal{K}_{xx} = \mathcal{K}_{yy} = 1/m$, $\mathcal{K}_{i \neq j} = 0$, and

$$\mathcal{K}_{zz} = \frac{1}{m_z^*} = \frac{2}{N} \sum_{\boldsymbol{k}} \frac{\mathrm{d}^2 \varepsilon_1(k)}{\mathrm{d}k_z^2} f(\bar{\varepsilon}(\boldsymbol{k}), T_\mathrm{e}). \tag{22}$$

If the electric field is applied along the z direction $\boldsymbol{E} = (0, 0, E)$, the average CM momentum, the drift velocity, and the frictional accelerations are all in the same direction: $\boldsymbol{p}_\mathrm{d} = (0, 0, p_\mathrm{d})$, $\boldsymbol{v}_\mathrm{d} = (0, 0, v_\mathrm{d})$, $\boldsymbol{A}_\mathrm{i} = (0, 0, A_\mathrm{i})$, and $\boldsymbol{A}_\mathrm{p} = (0, 0, A_\mathrm{p})$. The effective-force and energy-balance equations for the steady state then take the form

$$eE/m_z^* + A_\mathrm{i} + A_\mathrm{p} = 0 \tag{23}$$

$$eEv_\mathrm{d} - W = 0. \tag{24}$$

Here

$$v_\mathrm{d} = \frac{2}{N} \sum_{\boldsymbol{k}} v(k_z) f(\bar{\varepsilon}(\boldsymbol{k}), T_\mathrm{e}) \tag{25}$$

with $v(k_z) = \mathrm{d}\varepsilon_1(k_z)/\mathrm{d}k_z$, and

$$\tilde{\varepsilon}(\boldsymbol{k}) = \varepsilon_{\boldsymbol{k}_\parallel} + \varepsilon_1(k_z - p_\mathrm{d}). \tag{26}$$

Although this development can be applied in more general circumstances, we assume that the system considered here has a fixed carrier number density, independent of temperature. The chemical potential μ, involved in the Fermi distribution $f(\tilde{\varepsilon}(\boldsymbol{k}), T_\mathrm{e})$, is a function of T_e and Δ and is determined by (7). For the energy dispersion given by (19), this equation can be written as

$$\varepsilon_\mathrm{F}^0 = \frac{1}{\pi}\int_0^\Delta \mathrm{d}\epsilon \frac{\cos^{-1}(1-2\varepsilon/\Delta)}{\exp[(\varepsilon-\mu)/T_\mathrm{e}]+1} + \int_\Delta^\infty \frac{\mathrm{d}\varepsilon}{\exp[(\varepsilon-\mu)/T_\mathrm{e}]+1} \tag{27}$$

or

$$\frac{\varepsilon_\mathrm{F}^0}{T_\mathrm{e}} = \frac{1}{2\pi}\int_{-\pi}^{\pi} \mathrm{d}z \ln\left\{1+\exp\left[\frac{1}{T_\mathrm{e}}\left(\mu - \frac{\Delta}{2}(1-\cos z)\right)\right]\right\} \tag{28}$$

where

$$\varepsilon_\mathrm{F}^0 = \frac{\pi N_\mathrm{s}}{m} \tag{29}$$

is the zero-temperature Fermi energy of a pure two-dimensional system ($\Delta = 0$) with carrier sheet density N_s. The expressions for A_i, A_p and W are obtained by considering the z component of (8) and (9) with $v(\boldsymbol{k})$ replaced by $v(k_z)$ and $g(\boldsymbol{k},\boldsymbol{q})$ by $g(q_z)$ (equation (21)).

The expression (8) for the impurity-induced frictional acceleration A_i was obtained by assuming that the scattering centres are randomly distributed over the whole volume of the three-dimensional system. In a real superlattice system, however, one should take into account the modulation profile of the impurity density, such as background impurity, remote impurity, and interface roughness scatterings. Different expressions may be obtained and one may have a somewhat different temperature dependence of the frictional acceleration due to different types of elastic scatterings. Nevertheless, the effect of this difference is generally so small that we do not need to consider these details in the context of our present interest.

The effect of the carrier–carrier interaction is included in the expressions for A_i, A_p and W dynamically through the dielectric function $\epsilon(\boldsymbol{q},\omega)$ in the random-phase approximation. Dynamical screening may play a decisive role in specific problems, and thus must be taken into full account for each individual case. Nevertheless, it is now known that for a moderate carrier density of up to $\sim 10^{11}\,\mathrm{cm}^{-2}$, the dynamical effects of screening are not significant in most commonly encountered cases [16]. Therefore, to simplify the numerical process, in the present work we replace $\epsilon(\boldsymbol{q},\omega)$ in (8)–(10) by its static counterpart.

We have carried out numerical calculations for a model quantum-well superlattice system with well width a and period d. The form of the single-well function $\phi(z)$, which affects only the form factor $g(q_z)$, is not critical to the perpendicular transport properties. For convenience we simply choose $\phi(z) =$ constant inside the well and zero otherwise, such that

$$|g(q_z)|^2 = \left(\frac{\sin(q_z a/2)}{q_z a/2}\right)^2. \tag{30}$$

The material parameters of the system are chosen to correspond to the Γ-valley electrons in n-type GaAs-based superlattices: electron effective mass $m = 0.07\,m_e$ (m_e is the free electron mass), material mass density $\rho_d = 5.31\,\mathrm{g\,cm^{-3}}$, static dielectric constant $\kappa = 12.9$, optic dielectric constant $\kappa_\infty = 10.8$, longitudinal optic phonon frequency $\Omega_0 = 5.37 \times 10^{13}\,\mathrm{s^{-1}}$, acoustic deformation potential $\Theta = 8.5\,\mathrm{eV}$, piezoelectric constant $h_{14} = 1.41 \times 10^9\,\mathrm{V\,m^{-1}}$, longitudinal sound velocity $v_{sl} = 5.29 \times 10^5\,\mathrm{cm\,s^{-1}}$, and transverse sound velocity $v_{st} = 2.48 \times 10^5\,\mathrm{cm\,s^{-1}}$. We incorporate contributions from polar optic phonon scatterings, longitudinal acoustic phonon scatterings (deformation potential and piezoelectric couplings) and charged impurity scatterings. All these material parameters and the expressions for electron–phonon matrix elements are standard [17].

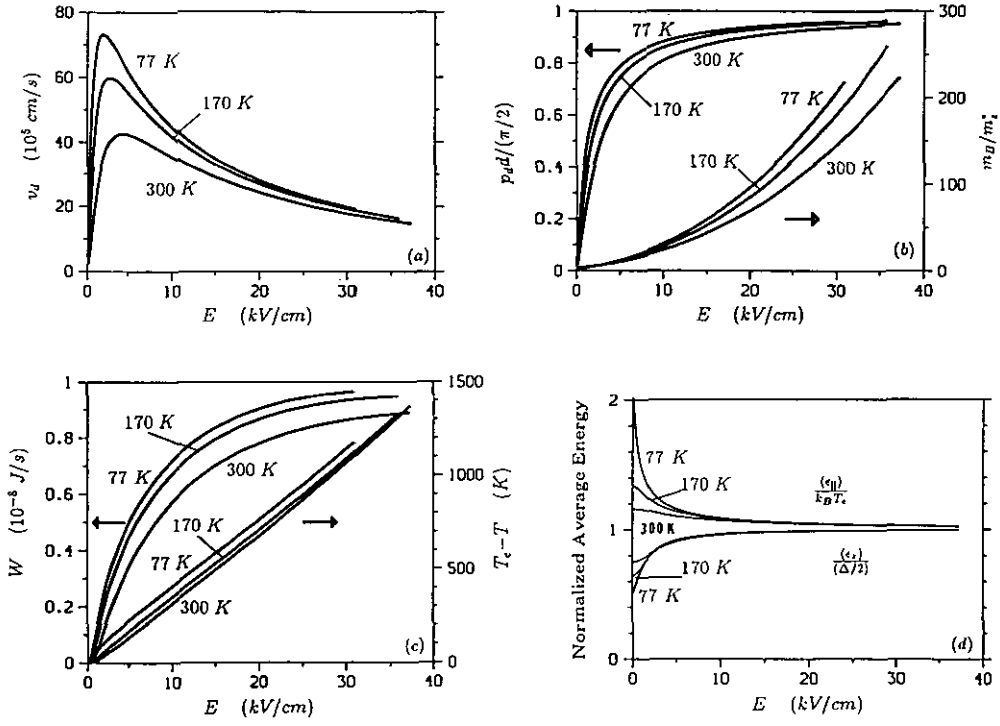

Figure 1. (*a*) Steady-state drift velocity v_d, (*b*) dimensionless CM momentum $p_d d$ and the average inverse effective mass $1/m_z^*$ normalized by $1/m_B$, (*c*) electron temperature $T_e - T$ and energy loss rate per carrier W, and (*d*) average transverse energy normalized by electron temperature $\langle\varepsilon_\parallel\rangle/k_B T_e$ and average longitudinal energy normalized by half-width of the miniband $\langle\varepsilon_z\rangle/(\Delta/2)$, are shown as functions of the applied electric field E at various lattice temperatures for a GaAs-based quantum-well superlattice system with $d = 100\,\text{Å}$, $a = 57\,\text{Å}$, $N_s = 4.0 \times 10^{11}\,\mathrm{cm^{-2}}$, miniband width $\Delta/k_B = 400\,\mathrm{K}$ and weak field mobility $\mu_0 = 2.0\,\mathrm{m^2\,V^{-1}\,s^{-1}}$ at 4.2 K. 1: $T = 77\,\mathrm{K}$, 2: $T = 170\,\mathrm{K}$, 3: $T = 300\,\mathrm{K}$.

In figure 1(*a*) we show the steady-state drift velocity v_d calculated using the balance equations (23) and (24), as a function of the electric field at lattice temperatures $T = 77\,\mathrm{K}$, $170\,\mathrm{K}$ and $300\,\mathrm{K}$, for perpendicular electron transport in a GaAs superlattice of $d = 100\,\text{Å}$, $a = 57\,\text{Å}$, electron sheet density $N_s =$

$4.0\times10^{11}\,\mathrm{cm}^{-2}$, miniband width $\Delta = 400\,\mathrm{K}$, and the impurity scattering rate is chosen to correspond to a low-temperature electron weak-field mobility $\mu_0 \simeq 2.0\,\mathrm{m}^2\,\mathrm{V}^{-1}\mathrm{s}^{-1}$. For this N_s, the zero-temperature Fermi energy is $\varepsilon_F \simeq 158.7\,\mathrm{K}$. The negative differential mobility behaviour is more pronounced at lower temperatures than at higher temperatures. To gain an appreciation of the parameters employed in the balance equation theory in figures 1(*b*) and (*c*) we plot the corresponding dimensionless CM momentum $p_d d$ and the electron temperature T_e as functions of the electric field E. In these figures the ensemble-averaged effective mass m_z^* (in units of $m_B \equiv \Delta d^2/2$) and energy transfer rate W (per carrier) are also shown as functions of E. We can see that $T_e - T$ increases with increasing E almost linearly, except for the low-field region ($E < 1\,\mathrm{kV\,cm}^{-1}$). The CM momentum $p_d d$, however, is highly non-linear. Values of $p_d d$ in the range $(0, \pi/2)$ are sufficient to describe the steady state, and thus it will saturate towards $\pi/2$ at high fields, which implies a positive but perhaps very large average effective mass.

The significant increase of the electron temperature with increasing electric field implies that the average electron longitudinal energy

$$\langle \varepsilon_z \rangle = \frac{2}{N} \sum_{k} \varepsilon_1(k_z) f(\bar{\varepsilon}(k), T_e) \tag{31}$$

will saturate towards $\Delta/2$ at high electric fields. On the other hand, the average transverse energy

$$\langle \varepsilon_\parallel \rangle = \frac{2}{N} \sum_{k} \varepsilon_{k_\parallel} f(\bar{\varepsilon}(k), T_e) \tag{32}$$

continues to increase with increasing electric field. At high fields, $\langle \varepsilon_\parallel \rangle \simeq k_B T$. This stands in contrast to the Monte-Carlo calculations [10–12], but is a consequence of the high electron temperature and the assumption that $\varepsilon_{k_\parallel}$ is parabolic. The calculated results for $2\langle \varepsilon_z \rangle/\Delta$ and $\langle \varepsilon_\parallel \rangle / k_B T_e$ are shown in figure 1(*d*).

4. Time dependence of the transient process

The balance equations (1) and (2) can be used to analyse the time development of the transient process if the timescale concerned is longer than the thermalization time of the system. In quantum wells, for example, the thermalization time appears to be very short [18]. Thus, in most cases we can expect these equations to describe the time-dependent process on a scale of the order of magnitude of 0.1 ps.

For the perpendicular transport configuration of carriers in a superlattice miniband as described in the preceding section, with a time-dependent uniform electric field $E(t)$ applied along the z direction, the balance equations (1) and (2) can be written as

$$\frac{\mathrm{d}v_d}{\mathrm{d}t} = \frac{eE(t)}{m_z^*} + A_i + A_p \equiv f_v(t, p_d, T_e) \tag{33}$$

$$\frac{\mathrm{d}h_e}{\mathrm{d}t} = eE(t)v_d - W \equiv f_e(t, p_d, T_e). \tag{34}$$

Here, the frictional accelerations A_i and A_p due to impurity and phonon scatterings, the energy loss rate to phonons W, as well as the average drift velocity v_d and the average electron energy h_e, are all functions of the centre-of-mass momentum p_d and the electron temperature T_e. In the transient process p_d and T_e are time dependent, and (33) and (34) describe the time evolution of these variables under the influence of the time-dependent field $E(t)$.

The drift velocity v_d, as a function of p_d and T_e, has been given by (25). Differentiating it with respect to time, we obtain

$$\frac{dv_d}{dt} = B_d\dot{p}_d + B_T\dot{T}_e \tag{35}$$

with

$$B_d = \frac{2d}{N}\sum_k v(k_z)[-f'(\bar{\varepsilon}(k), T_e)]\frac{\Delta}{2T_e}\sin(k_z - p_d)d = \frac{1}{m_z^*} \tag{36}$$

$$B_T = \frac{2}{N}\sum_k v(k_z)[-f'(\bar{\varepsilon}(k), T_e)]\left[\frac{\bar{\varepsilon}(k)}{T_e^2} + \frac{d}{dT_e}\left(\frac{\mu}{T_e}\right)\right]. \tag{37}$$

The kinetic part of the average electron energy, $\langle\varepsilon\rangle$, is just the sum of $\langle\varepsilon_\parallel\rangle$ and $\langle\varepsilon_z\rangle$ given by (31) and (32)

$$\langle\varepsilon\rangle = \frac{2}{N}\sum_k \varepsilon(k) f(\bar{\varepsilon}(k), T_e) \tag{38}$$

which depends on both p_d and T_e, leading to

$$\frac{d\langle\varepsilon\rangle}{dt} = C_d\dot{p}_d + C_T\dot{T}_e \tag{39}$$

with

$$C_d = \frac{2d}{N}\sum_k \varepsilon(k)[-f'(\bar{\varepsilon}(k), T_e)]\frac{\Delta}{2T_e}\sin(k_z - p_d)d = v_d \tag{40}$$

$$C_T = \frac{2}{N}\sum_k \varepsilon(k)[-f'(\bar{\varepsilon}(k), T_e)]\left[\frac{\bar{\varepsilon}(k)}{T_e^2} + \frac{d}{dT_e}\left(\frac{\mu}{T_e}\right)\right]. \tag{41}$$

The contribution of the intercarrier Coulomb interaction to the average electron energy is independent of p_d and thus it induces only an ordinary specific heat modification to the coefficient C_T. For simplicity we omit this modification in the following numerical calculations.

The differential equations which will be employed to analyse the time evolution of p_d and T_e are

$$B_d\dot{p}_d + B_T\dot{T}_e = f_v(t, p_d, T_e) \tag{42}$$

$$C_d\dot{p}_d + C_T\dot{T}_e = f_e(t, p_d, T_e). \tag{43}$$

Starting from initial values of p_d and T_e we obtain the transient response of p_d and T_e, and thus all the physical quantities v_d, m_z^*, ..., to a given applied field $E(t)$, by solving this set of differential equations.

We have carried out many numerical calculations of miniband transient transport for various GaAs-based quantum-well superlattices. Electrons, phonons, material parameters and electron–phonon coupling constants are the same as those used in the steady-state calculation of the preceding section.

In figure 2 we plot the transient response of the drift velocity v_d to step electric fields of various strengths (E = 0.3, 0.7, 2.0, 5.0 and 10.0 kV cm^{-1}) at a lattice temperature T = 77 K for a quantum-well superlattice with d = 57 Å, a = 37 Å, $N_s = 2.0 \times 10^{10}$ cm^{-2}, Δ = 400 K and low-temperature impurity-limited weak-field mobility μ_0 = 20 m^2 V^{-1} s^{-1}. For this carrier-sheet density the zero-temperature Fermi energy is only ε_F^0 = 7.9 K, much lower than that of the system described in figure 1. In the case of E = 0.3 kV cm^{-1} and E = 0.7 kV cm^{-1}, the response is qualitatively similar to that of parallel transport in GaAs heterosystems [19]: v_d rises monotonically with a time constant of 1.5–3 ps, without overshoot. When the field increases into the negative differential mobility regime of the steady-state curve (figure 2 inset), the drift velocity overshoot appears. With a continuing increase of field strength, the drift velocity overshoot becomes more pronounced and the instantaneous peak velocity is reached at an earlier time. In the case of E = 10 kV cm^{-1} the transient peak drift velocity is about 2.5 times that of the steady-state value, and this peak velocity is reached at about t = 0.18 ps after turn-on of the electric field.

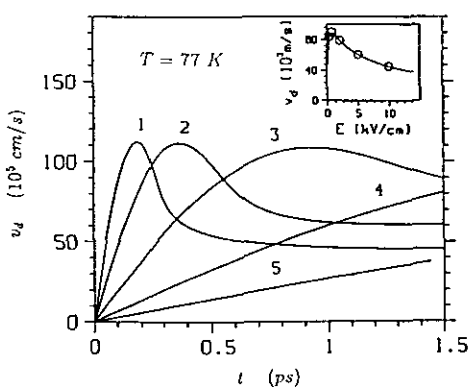

Figure 2. Calculated transient response of the drift velocity v_d to step electric field turned on at time t = 0 with various field strengths. 1: 10 kV cm^{-1}, 2: 5.0 kV cm^{-1}, 3: 2.0 kV cm^{-1}, 4: 0.7 kV cm^{-1}, 5: 0.3 kV cm^{-1}. The inset shows the corresponding locations of these fields on the steady-state velocity-field curve. The lattice temperature is T = 77 K. The system is an n-type GaAs-based quantum-well superlattice with period d = 57 Å, electron sheet density $N_s = 2.0 \times 10^{10}$ cm^{-2}, miniband width Δ/k_B = 400 K and low-temperature impurity-limited mobility μ_0 = 20 m^2 V^{-1} s^{-1}.

In regard to the temporal development of the electron temperature T_e, the centre-of-mass momentum p_d and the average inverse effective mass $1/m_z^*$, we exhibit results in figure 3 for T_e, p_d and $1/m_z^*$, as well as v_d, as functions of time for the same system as that described in figure 2 with the step electric field strengths E = 10 kV cm^{-1}, and E = 5 kV cm^{-1}, respectively. It should be noted that the momentum p_d, the ensemble averaged inverse effective mass $1/m_z^*$, and the drift velocity v_d, all refer to the collective response of the system for all carriers in the

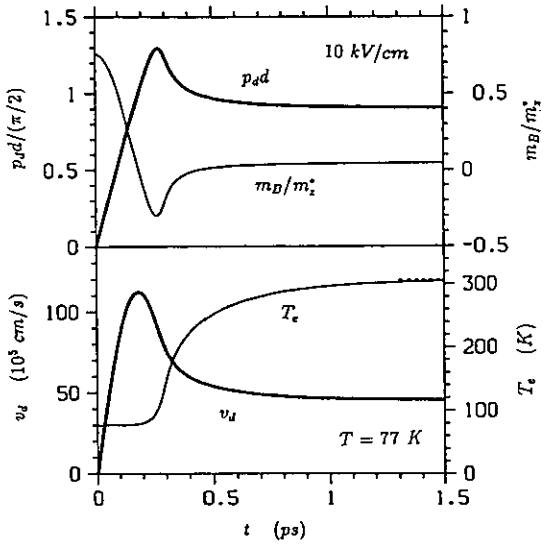

Figure 3. Time development of the drift velocity v_d, electron temperature T_e, normalized CM momentum $p_d d$, and normalized average inverse effective mass m_B/m_z^* ($m_B \equiv \Delta d^2/2$ is the perpendicular band electron mass at the miniband bottom). The system is the same as that described in figure 1, with a step field strength $E = 10\,\mathrm{kV\,cm^{-1}}$ at a lattice temperature of $T = 77\,\mathrm{K}$.

energy band. In the steady state, the drift velocity v_d must be in the same direction as the applied field (for the case discussed in this paper) so that the energy flows into the electron system from the field. Therefore, the steady-state value of p_d never exceeds $\pi/2d$, and the average inverse effective mass is always positive, (as shown in figure 1), notwithstanding that individual electrons driven beyond the inflection point may sense a negative inverse effective band mass. In the case of transient response, however, the electric field can drive p_d beyond $\pi/2d$ and $1/m_z^*$ can become negative in a limited time interval, as shown in figure 3 for the time range $0.19 < t < 0.44\,\mathrm{ps}$, and in figure 4 for the time range $0.34 < t < 0.72\,\mathrm{ps}$. The instantaneous peak drift velocity is reached at $t = 0.18\,\mathrm{ps}$ in figure 3, and at $t = 0.37\,\mathrm{ps}$ in figure 4. This reflects the fact that the electric field acceleration is responsible for the rapid increase of the drift velocity following start-up, and contributes to its decrease within the time intervals indicated above, manifesting a genuine Bloch-type behaviour for a non-parabolic band. This phenomenon is more pronounced at lower temperatures and at lower impurity scattering rates than at higher ones. In figure 5 we exhibit the response of v_d, T_e, p_d and $1/m_z^*$ to a step field of strength $E = 20\,\mathrm{kV\,cm^{-1}}$ at $T = 300\,\mathrm{K}$ for a GaAs-based quantum-well superlattice system of $d = 57\,\text{Å}$, $a = 37\,\text{Å}$, $N_s = 2 \times 10^{10}\,\mathrm{cm^{-2}}$, $\Delta = 400\,\mathrm{K}$ and low-temperature impurity-limited mobility $\mu_0 = 2.0\,\mathrm{m^2\,V^{-1}\,s^{-1}}$.

In order to achieve a broader perspective on transient response phenomena, we consider the case of an impulsive external electric field, which is turned on at $t = 0$ and is maintained at a constant value until being turned off after a short time interval Δt. Following shut-down of the field, the carriers relax from the current-carrying state at time $t = \Delta t$ in the absence of the driving force. Since the current-carrying state, which embodies the initial conditions for the relaxation process, is sensitive

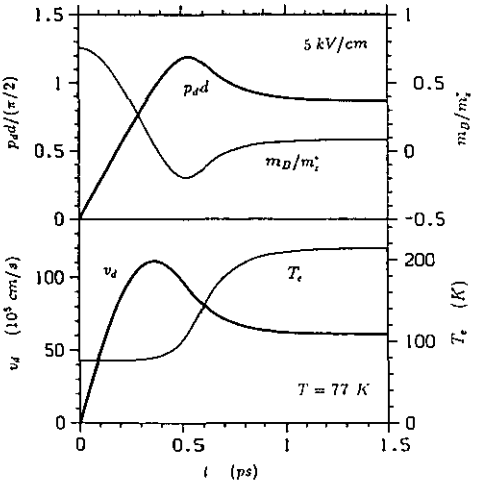

Figure 4. Same as figure 3, but with step field strength $E = 5.0\,\mathrm{kV\,cm^{-1}}$ and at lattice temperature $T = 77\,\mathrm{K}$.

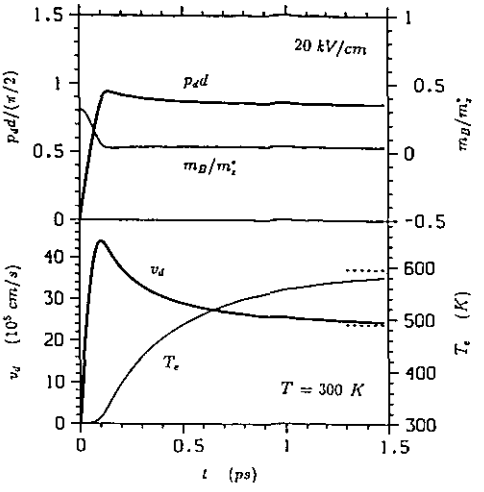

Figure 5. Same as figure 3, but with step field strength $E = 20\,\mathrm{kV\,cm^{-1}}$ and at lattice temperature $T = 300\,\mathrm{K}$.

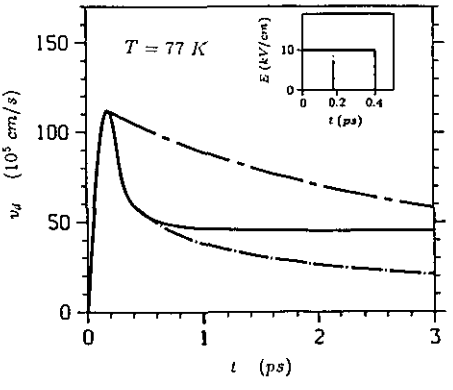

Figure 6. Transient response of the drift velocity v_d to a 0.18 ps impulse electric field (chain curve) and to a 0.4,ps impulse electric field (broken curve), in comparison with v_d response to a step field of the same strength, $E = 10\,\mathrm{kV\,cm^{-1}}$. The system is the same as that described in figure 1. The lattice temperature is $T = 77\,\mathrm{K}$.

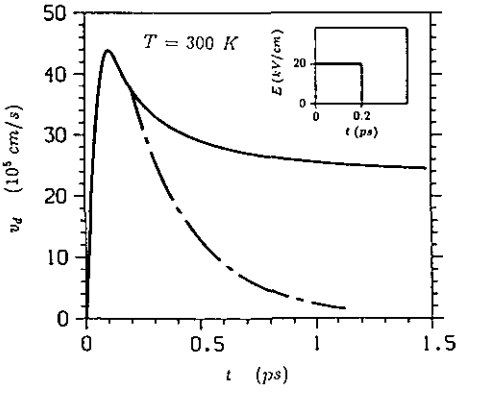

Figure 7. Transient response of the drift velocity v_d to a 0.2 ps impulse electric field (broken curve) and to a step field of the same strength, $E = 20\,\mathrm{kV\,cm^{-1}}$. The system is the same as that described in figure 4. The lattice temperature is $T = 300\,\mathrm{K}$.

to the field-duration interval Δt, the ensuing relaxation behaviour is also sensitively dependent upon the impulse interval. In figure 6 we show the response of the same superlattice system as that described in figure 2 to an 0.18 ps impulse electric field, to a 0.4 ps electric field, and to a step electric field, all of the same strength of $E = 10\,\mathrm{kV\,cm^{-1}}$. At $t = 0.18\,\mathrm{ps}$ after the electric field is turned on the drift velocity achieves its peak value while the system has not yet been heated significantly ($T_e = 78.9\,\mathrm{K}$), and thus it suffers relatively light scattering due to phonons. This

results in a relatively long time for it to relax to the final state upon field turn-off at 0.18 ps. Despite the fact that the system will ultimately approach a zero drift-velocity state, it surprisingly maintains a much higher drift velocity in the relaxation process than that for a continuously applied field over a considerable time range. This unusual phenomenology is a consequence of the fact that the field drives the centre of mass to a lower velocity in the time interval 0.19–0.42 ps, due to a negative inverse effective mass, a feature unique to non-parabolic band transport. In delaying the shut-off of the electric field to $t = 0.42$ ps, however, the system becomes hotter ($T_e = 231$ K) and thus suffers stronger phonon scattering, leading to a shorter relaxation time to the final state. With stronger impurity scattering ($\mu_0 = 2.0\,m^2\,V^{-1}\,s^{-1}$) and at higher lattice temperature $T = 300$ K (stronger phonon scattering) the average inverse effective mass remains positive in the temporal development of the relaxation process even with a field of $20\,kV\,cm^{-1}$, leading to substantially diminished drift velocities in pulse relaxation, below continuous field values. Figure 7 illustrates this shorter relaxation time.

5. Conclusions

In this paper we have carried out a systematic analysis of hot-carrier Bloch transport in a superlattice miniband based upon the balance-equation approach of Lei and Ting, extended to an arbitrary energy band structure. In its focus on the centre-of-mass motion, the balance equation approach addresses the collective response of the carrier system, rather than tracing out individual electron motions. The key quantity in describing non-parabolic systems is the ensemble-averaged inverse effective mass $1/m_z^*$, that governs the dynamics of the centre of the mass as a single particle with charge Ne and variable mass Nm_z^* through a Newtonian equation of motion which includes the driving force (field) acceleration and the frictional accelerations due to impurity and phonon scatterings. This dynamical force-balance equation, together with the dynamical energy-balance equation, provides the basis for a succinct determination of steady-state and transient transport in a superlattice miniband.

In the case of steady-state transport the velocity-field curve exhibits negative differential mobility for all the miniband widths, carrier sheet densities and lattice temperatures examined. This effect is more pronounced at lower lattice temperatures and for wider minibands, as long as the tight-binding description remains adequate. The peak drift velocity v_p and the threshold field E_c depend strongly on the miniband width Δ, the lattice temperature T and the impurity scattering rate.

For a step electric field having a strength within the range of negative differential steady-state mobility the transient current exhibits a very pronounced overshoot. In GaAs systems the instantaneous peak drift velocity can be three times that of the steady-state value, and is generally reached within 0.12–0.3 ps after turning on an electric field of $10\,kV\,cm^{-1}$. It is of special interest to note that the ensemble-averaged inverse effective mass can be driven by the field into the range of negative values. In consequence of this, if the electric field is shut down just before the inverse effective mass becomes negative, the drift velocity will maintain a higher value than it would have without shut-down of the field, before it ultimately relaxes to zero. These striking results realistically exemplify genuine Bloch-type transport.

Further theoretical and experimental explorations of steady-state and time-dependent miniband-electron transport should provide intriguing insight into physical

processes of key interest, such as Bloch oscillations, for semiconductor superlattice systems.

Acknowledgment

The authors would like to express their thanks to the NEC Research Institute, Princeton, New Jersey, USA for the support of this work.

References

[1] Esaki L and Tsu R 1970 *IBM J. Res. Dev.* **14** 61
[2] Esaki L and Chang L L 1974 *Phys. Rev. Lett.* **33** 495
[3] Davies R A, Kelly M J and Kerr T M 1985 *Phys. Rev. Lett.* **55** 1114
[4] Choi K K, Levine B F, Malik R J, Walker J and Bethea C G 1987 *Phys. Rev.* B **35** 4172
[5] Deveaud B, Shah J and Damen T C 1987 *Phys. Rev. Lett.* **58** 2582
[6] Sibille A, Palmier J F, Wang H and Mollot F 1990 *Phys. Rev. Lett.* **64** 52
[7] Sibille A, Palmier J F, Minot C and Mollot F 1989 *Appl. Phys. Lett.* **54** 265
Sibille A, Palmier J F, Mollot F, Wang H and Esnault J C 1989 *Phys. Rev.* B **39** 6272
Sibille A, Palmier J F, Wang H, Esnault J C and Mollot F 1989 *Solid State Electron.* **32** 1461
[8] Grahn H T, von Klitzing K, Ploog K and Döhler G H 1991 *Phys. Rev.* B **43** 12094
[9] Lebwohl P A and Tsu T 1970 *J. Appl. Phys.* **91** 2664
[10] Price P J 1973 *IBM J. Res. Dev.* **17** 39
[11] Andersen D L and Aas E J 1973 *J. Appl. Phys.* **44** 3721
[12] Artaki M and Hess K 1985 *Superlatt. Microstruct.* **1** 489
[13] Lei X L 1992 *Phys. Status Solidi b* **170** 519
[14] Lei X L and Ting C S 1985 *Phys. Rev.* B **32** 1112
[15] Lei X L, Horing N J M and Cui H L 1991 *Phys. Rev. Lett.* **66** 3277
[16] Shah J 1989 *Solid State Electron.* **32** 1051
[17] Lei X L, Birman J L and Ting C S 1985 *J. Appl. Phys.* **58** 2270
[18] Knox W H, Chemla D S, Livescu G, Cunningham J E and Henry J E 1988 *Phys. Rev. Lett.* **61** 1290
[19] Lei X L, Cui H L and Horing N J M 1987 *J. Phys. C: Solid State* **20** L287